

Excitation of Giant Surface Waves During Laser Wake Field Acceleration

Travis Garrett,¹ Christopher Pieronek,¹ E. Rockafellow,² Oliver Sale,³ Sahir Virani,¹ J. E. Shrock,² B. Miao,² A. Sloss,² Jennifer Elle,¹ and H. M. Milchberg²

¹*Air Force Research Laboratory, Directed Energy Directorate, Albuquerque, NM 87123, USA*

²*Institute for Research in Electronics and Applied Physics and Department of Physics, University of Maryland, College Park, Maryland 20742, USA*

³*Leidos Innovations Center, Albuquerque, NM 87106, USA*

We have detected the presence of very high intensity surface waves that are excited during plasma waveguided laser wakefield acceleration. Wakefield acceleration can be enhanced by the introduction of an “all optical” plasma waveguide that confines and guides a laser pulse at the optimal intensity over long distances, producing quasimonoenergetic multi-GeV electron bunches. However strong pulses of radio frequency radiation (RF) are also produced, and particle in cell simulations show why: a continuous stream of multi-MeV electrons are also ejected radially from the plasma due to nonlinear wave breaking, and these excite and copropagate coherently with a giant cylindrical Sommerfeld surface wave. Laboratory measurements, simulations, and analytic approximations all converge on a 20 J laser pulse exciting a 1 Joule, 400 GW broadband THz surface wave, with a peak electric field strength of 35 GV/m.

The invention of chirped pulse amplification and high intensity femtosecond scale laser pulses [1–4] have stimulated many scientific disciplines and applications [5–11], including laser wakefield acceleration (LWFA) [12], atmospheric filamentation [13, 14], and the generation of strong broadband THz radiation [15–17]. We report in this letter on the discovery that very high intensity surface waves are excited during plasma waveguided LWFA [18, 19], in close analogy to a process that occurs during femtosecond filamentation [20–23]. Simulations and experiments show that these surface waves (surface plasmon polaritons (SPP) [24, 25] on a plasma substrate) are an intense source of THz radiation, as they convert a significant fraction of the laser energy into a broadband THz pulse.

The key idea behind the original proposal for LWFA [26] is that plasmas can support very large accelerating fields ($|E| \sim 100$ GV/m), some 10^3 times greater than in traditional LINACs. In the simplest setup for LWFA, a sufficiently energetic short pulse laser is focused into a short gas jet and undergoes relativistic self-focusing in the generated plasma, reaching the intensity threshold for ponderomotively expelling electrons from the center of the pulse and generating a relativistic plasma wave or wakefield, whose axial electrostatic field accelerates electrons loaded into the wake via self-injection and wave-breaking. The long distance co-propagation of the injected electrons with the strong wake fields boosts them to GeV energy scales (in contrast to the \sim MeV energies within the laser pulse).

The addition of a plasma waveguide [19, 27–32] improves the LWFA process by providing a fiberoptic-like channel that captures the laser pulse near its beam waist and maintains that intensity over many Rayleigh lengths. In the first “all optical” plasma waveguide-based multi-GeV accelerator [32] an initial Bessel beam laser pulse was used to rapidly generate and heat a long thin col-

umn of plasma in an extended supersonic hydrogen gas jet. The resulting axially extended cylindrical shock wave expands into the surrounding neutral gas, producing a low density plasma core surrounded by a higher density radial shell of neutral gas. In that experiment and those of this paper, the primary LWFA drive pulse (typically with normalized vector potential $a_0 \sim 2$ and pulsewidth < 100 fs) is injected into the end of this prepared refractive index structure after a delay of several nanoseconds. The radial wings in the very early leading edge of the pulse fully ionizes the inside of the shock wall, forming a plasma waveguide on the fly, that confines the remainder of the pulse. Nitrogen gas can then be added at axial locations along the plasma column to enable ionization injection [33–35] at those positions and subsequent acceleration. Recent experiments have confirmed the promise of this technique [36] with electron bunches being accelerated to ~ 10 GeV [37, 38].

A significant side effect has also appeared during these successful waveguided LWFA experiments: the generation of unusually intense pulses of RF. This radiation has been strong enough to temporarily incapacitate or permanently damage a wide range of electronic lab instrumentation including computers, motion controllers, oscilloscopes, and vacuum pumps. It has been previously noted that intense THz pulses can be produced via transition radiation as the electron beams exit the end of the plasma column [39–41]. However, this new intense RF is still generated during when the N₂ gas is removed and no GeV electrons are produced. In this letter we present new measurements of this intense RF taken during LWFA experiments at the ALEPH facility [42], and show that a novel surface wave phenomenon explains their generation.

Recent experiments and theory on RF generation during femtosecond filamentation [21–23, 43–46] shed light on the LWFA physics. Electrons in a filamentation

plasma retain some kinetic energy after the laser pulse has passed, typically 1-10 eV depending on the laser parameters. The hot tail of the distribution expands diffusively from the boundary of the plasma into the surrounding atmosphere, thus producing radial current pulse J_r [20]. The amplitude and spectrum of J_r are set by the electron energies, an E_r field that grows in response to the current, and electron-neutral collisions [22].

Particle in cell (PIC) simulations [47, 48] reveal that the J_r current pulse excites a SPP on the outer boundary of the plasma column [22], in particular a transverse magnetic Sommerfeld wave [49–54] given the cylindrical symmetry (see also [55, 56]). The relatively low frequency content of J_r excites SPPs that are well below the cutoff frequency (which is close to the plasma frequency ω_{pl} , ~ 1 THz for $n_e \sim 3 \times 10^{22} \text{ m}^{-3}$) and their group velocity is thus almost c . The J_r current pulse also translates at nearly c behind the laser pulse, and it thus co-propagates coherently with the surface wave, driving its intensity higher until it saturates. At the end of the plasma column most of the surface wave detaches [57, 58], becoming forward directed free space RF (a time reversal of [59]), while a fraction of the energy is reflected and travels back up the plasma.

Like filamentation, LWFA also ionizes cylindrical volumes of plasma (density $n_e \sim 10^{23} \text{ m}^{-3}$) that grow longer at almost c , and imparts the electrons with an initial velocity distribution. However the laser E field strength is roughly 10^3 times stronger during LWFA, and the typical electron energies thus 10^6 higher. Most of these MeV scale electrons remain confined within the plasma, comprising the Langmuir oscillation, but previous PIC simulations [60, 61] demonstrate that a subset of them are ejected radially from the plasma. As these electrons exit the plasma they will drive a far stronger J_r current pulse, and excite a much more intense surface wave.

The Sommerfeld solution has nonzero E_r , E_z and B_ϕ fields, which have Bessel function profiles inside a cylindrical plasma of radius r_{pl} , and Hankel function scaling outside. We measure E_r outside the plasma, where the analytic solution is given by:

$$E_r(r, z, t) = -\frac{\pi r_{pl} E_0}{2r_{outer}} e^{i(\omega t - h z)} H_1^{(1)}(\gamma_{air} r), \quad (1)$$

with angular frequency ω , and $H_1^{(1)}$ is a Hankel function of the first kind with order 1. The parameter γ_{air} is given by $\gamma_{air}^2 = k_0^2 - h^2$, where $k_0 = \omega/c$ is the free space wave number, $\text{Re}(h)$ is the SPP wavenumber and $1/\text{Im}(h)$ sets an attenuation length scale L_{decay} . We define an outer length scale $r_{outer} = 1/|\gamma_{air}|$: for radii $r_{pl} < r < r_{outer}$ the Hankel function is approximately $H_1^{(1)} \simeq -2r_{outer}/(\pi r)$, and for $r > r_{outer}$ it smoothly transitions to an exponential fall off. E_0 is the peak wave amplitude at the surface of the plasma $r = r_{pl}$.

The parameter γ_{air} is found by matching the internal

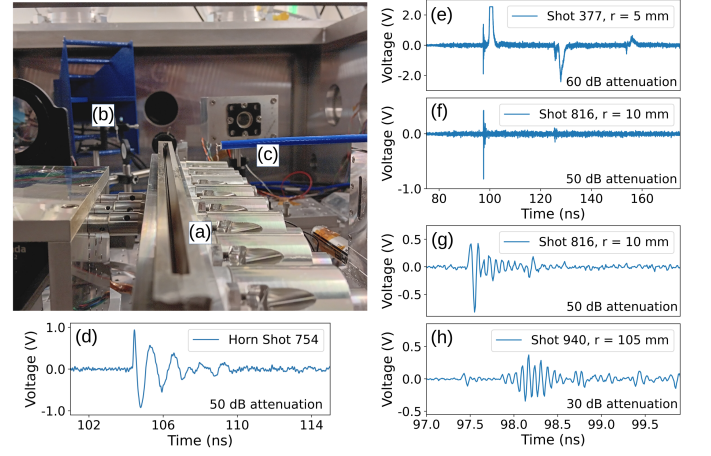


FIG. 1. (a) Down axis view of the gas jet in the LWFA vacuum chamber, at the ALEPH facility. (b) Downstream broadband RF horn. (c) Coax cable converted into a D-dot probe, on a stage that can vary the radius r from 0 to 105 mm from the plasma that forms above the gas jet. (d) Example signal recorded by RF horn, confirming presence of strong RF radiation. (e) Example signal recorded at a distance of $r = 5$ mm from the plasma. In addition to the electromagnetic pulse, a large monopole signal is observed. (f) Example signal recorded at $r = 10$ mm during a H2 only run. A strong transient electromagnetic pulse is still generated. (g) Zoom in on the transient RF pulse shown in (f). An inverted pulse is seen 0.7 ns after the main pulse, which may be due to reflections after the main SPP detaches from the plasma. (h) Zoom in on an example signal recorded at the largest separation $r = 105$ mm. At this distance the initial broadband pulse is small compared to the ensuing reflected waves.

Bessel function field profiles to the external Hankel functions. Historically a variety of solutions have been developed via simplifying assumptions, but the full equations can be solved using an iterative method [23, 52]. With an initial guess of $\gamma_{air}^{N=1} = 0.5k_0$ the subsequent iterations are given by:

$$\gamma_{air}^{N+1} = \frac{\gamma_{pl}^N H_1^{(1)}(\gamma_{air}^N r_{pl}) J_0(\gamma_{pl}^N r_{pl})}{\varepsilon_{pl}(\omega) H_0^{(1)}(\gamma_{air}^N r_{pl}) J_1(\gamma_{pl}^N r_{pl})}, \quad (2)$$

with $\gamma_{pl}^N = \sqrt{(\gamma_{air}^N)^2 + (\varepsilon_{pl}(\omega) - 1)k_0^2}$, and plasma permittivity $\varepsilon_{pl}(\omega) = 1 + \omega_{pl}^2/(i\omega\nu - \omega^2)$. The iterative solve typically converges in 10-30 steps [62], thus yielding r_{outer} as a function of r_{pl} , n_e and ω . Unlike filamentation we assume the electron collision frequency ν is approximately zero. The electrons at the outer plasma radius are initially ionized with low energies, but the subsequent arrival of the LWFA SPP will accelerate them to $\sim 1/3$ of the speed of light, in which case both the electron-ion and electron-neutral momentum transfer collision frequencies are negligible.

A well matched laser pulse can maintain a stable $a_0 \sim 2$ over 10 cm [36], providing a consistent stream of expelled electrons that steadily amplify the Sommerfeld

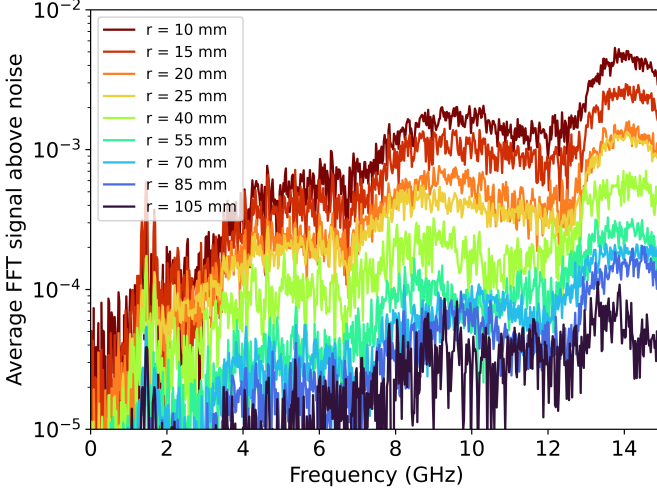


FIG. 2. Average FFTs as a function of D-dot separation from the plasma column, ranging from 10 mm to 105 mm. In general there is an approximately linear ramp up in frequency, with additional multi-GHz bumps due to reflections off of the gas jet, and a rapid fall off with increasing separation.

surface wave. Over time the field strength will saturate (setting the asymptotic E_0 value) as it drives counteracting currents, which occurs roughly when the high energy expelled electrons ($K_{\text{eV,max}}$) are bound by the $1/r$ field. For electrons expanding out to r_{max} before returning to the plasma, the asymptotic surface field strength E_0 is approximately:

$$E_0 = K_{\text{eV,max}} / (r_{\text{pl}} \ln(r_{\text{max}}/r_{\text{pl}})). \quad (3)$$

For instance, $K_{\text{eV,max}} = 10$ MeV electrons that expand out $r_{\text{max}} \sim 5$ mm yields $E_0 \sim 35$ GV/m, in good agreement with the simulations seen in Figs 4 and 5.

With lessons from the filamentation radiation in mind we took measurements of the RF generated during plasma waveguided LWFA at the ALEPH facility. Initial measurements inside the vacuum chamber were taken with a broadband RF horn (Fig 1), which confirmed that very intense pulses of RF were being generated, with the same radial polarization seen during filamentation [22]. We then focused on measuring surface waves in the vicinity of the plasma column, adapting the technique developed for filamentation [23]. A coax cable was converted into a D-dot probe, and placed near the midpoint of the plasma column on a motorized stage that could scan in the radial direction, ranging from 0 mm away from the plasma to 105 mm. The combination of the internal coax, vacuum feed-through, and external coax were characterized with a Rohde and Schwarz Vector Network Analyzer (VNA) to determine the frequency dependent transmission loss from the D-dot to the oscilloscope.

As with the horn, very large transient pulses were detected, and strong attenuators were added between the coax and the oscilloscope, ranging from 60 dB at the

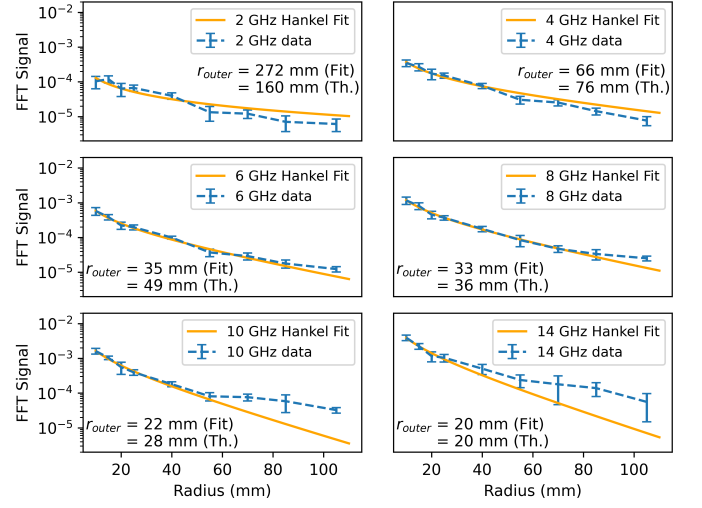


FIG. 3. FFT signal in different frequency bins as a function of radius, and fit to the expected Hankel function profile (which scales as $\sim 1/r$ for $r < r_{\text{outer}}$ and $\sim e^{-r}$ for $r > r_{\text{outer}}$). The data fit values (Fit) for the outer length scale r_{outer} are quite close to the theoretical (Th.) predictions as given by (2) for a plasma column with radius $r_{\text{pl}} = 70 \mu\text{m}$ and electron density $n_e = 2 \times 10^{23} \text{ m}^{-3}$.

smallest separations to 30 dB at the largest. In addition to the strong electromagnetic signals, at close separations ($r = 5$ mm) large monopole signals were frequently detected (along with subsequent coax reflections): see Fig 1. We suspect at this distance that transversely expelled electrons are directly colliding with the D-dot probe and depositing charge in the metal core, resulting in a monopole pulse as the charge returns to ground. In addition to this unexpected signal, the noise floor in the recorded traces rise in amplitude about 20 ns before the primary signal arrives: this may be due to a x-ray background that begins arriving at the oscilloscope before the RF signal which travels along the curved coax line.

At larger radial separations (Fig 1) the monopole signal disappears, leaving only the sharp electromagnetic transient. This transient pulse is excited whether Nitrogen is added to the gas or not, although the amplitude is larger on average when it is included. Zooming in we see the primary pulse is broadband, and it is consistently followed by a smaller inverted secondary pulse about 0.7 ns later, which is consistent with some reflected waves returning back upstream after the primary SPP detaches from the end of the plasma. As we progress out to larger radii the primary signal amplitude falls off significantly (we reduce the amount of attenuation to preserve resolution), and by $r = 105$ mm the subsequent reflected waves are significantly louder than the primary.

We next take FFTs of the oscilloscope traces. Given the relative magnitude of the later reflections at large radii, we truncate the time series data 0.5 ns after the primary pulse is detected (the precise form of the trun-

cation doesn't significantly change the results). We also use the quiescent first half of the truncated time data as a measure of the noise, and subtract this from the second half which contains the pulse. Averaging the FFTs together for all shots taken at the same radius (and adjusting for varying attenuation) yields Fig 2. In general the spectra ramp up roughly linearly with increasing frequency, which is consistent with the RF signal being the low frequency tail of a high frequency broadband pulse, and they also fall off quickly with increasing radius. Additional multi-GHz bumps can be seen on top of the linear trend, which are likely due to reflections off of the gas jet assembly below the plasma, while the spike below 2 GHz stems from a resonance in the D-dot probe.

The FFTs are then split into 2 GHz bins and averaged, and then plotted as a function of radius, see Fig 3. In general these are very well fit by the expected Hankel function dependence (1), as was the case during filamentation [23]. The fit values for the r_{outer} parameter are also very close, both in overall magnitude and frequency scaling, to the predictions given by (2) for a plasma with our plasma parameters. We note that there is extra signal at large radii for the higher frequencies, which is consistent with free radiation being excited by the J_r current pulse in addition to the surface wave [56].

The excellent agreement of the measured radial profiles with the Sommerfeld SPP predictions supports the view that energetic electron currents are exciting a giant SPP. We next perform electromagnetic PIC simulations [47, 48, 63–65] of the LWFA process, using the ICEPIC code [66] with moving window reference frame that tracks the laser pulse. A linearly polarized 20 J, 800 nm, 65 fs FWHM Gaussian laser pulse with a $30\ \mu\text{m}$ beam waist is driven into a $70\ \mu\text{m}$ radius plasma waveguide (see Fig 4) where the radial profile is determined by hydrodynamic simulations of the Bessel beam driven cylindrical shock wave [67]. The plasma waveguide does an excellent job of smoothly guiding the pulse and holding its intensity and shape nearly constant over 5 ps of evolution, driving a blow out bubble in its wake. Critically, nonlinear plasma wave breaking [12, 68, 69] at the end of the first bubble consistently ejects a cone of MeV scale electrons out of the plasma column, with a peak kinetic energy $K_{\text{eV,max}}$ of 10 MeV: see Fig 4. Wave breaking can also be seen expelling lower energy electron jets from the subsequent Langmuir oscillations. The radial current pulse J_r contained in these conical jets excites a massive Sommerfeld SPP (seen in red in Fig 4, with a field strength of $\sim 20\ \text{GV/m}$ at 5 ps), which grows steadily larger with propagation distance.

In contrast to other LWFA simulations where the transverse ejection of electrons is more sporadic, the stabilization of the laser pulse by the plasma waveguide also stabilizes the ensuing plasma oscillations, leading to highly regular and energetic wave breaking. The peak energy of the ejected electrons grows rapidly with increasing

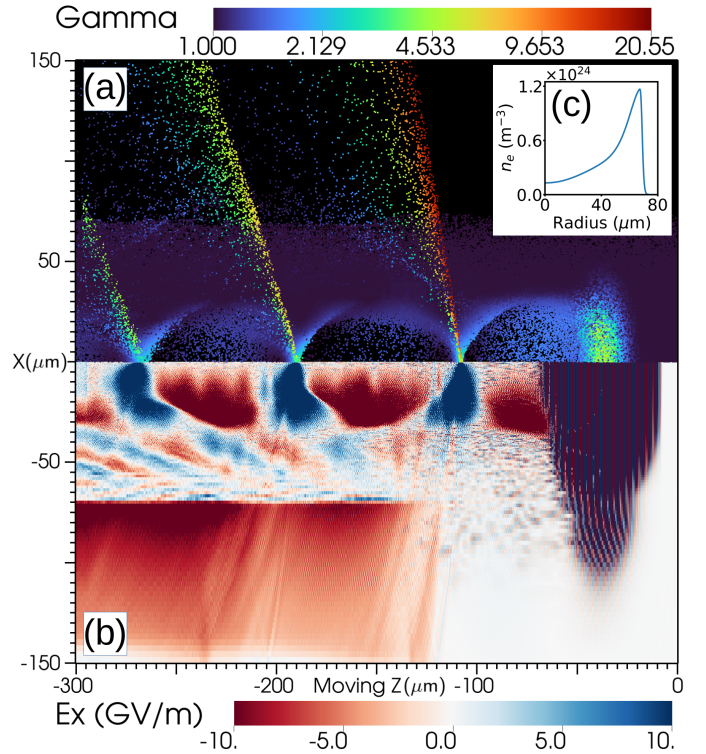


FIG. 4. (a) 2D slice of electron γ from a 3D PIC simulation of plasma waveguided 20 J LWFA, with the $w_0 = 30\ \mu\text{m}$ beam waist matched to the waveguide. 10 MeV electrons are being ejected from the plasma to nonlinear wave breaking. (b) E_x field strength from the same simulation, where the color scale has been set to show the strong THz SPP (red) growing on the outer boundary of the plasma. After 5 ps of propagation (1.5 mm), the peak SPP E field has grown to almost 20 GV/m. (c) Radial profile of plasma number density that defines the waveguide.

a_0 , and at higher values the ponderomotive force directly expels charge as well. At lower $a_0 < 1$ values the clean wave breaking at the end of the first oscillation disappears, but returns in a turbulent form in later oscillations due to increasing wavefront curvature [69].

The 3D LWFA simulations are computationally expensive, so we have also performed large scale 2D \hat{r} - \hat{z} axisymmetric PIC simulations within the same plasma waveguide. The laser pulse is replaced with a particle beam (traveling at $\gamma = 120$) that has been tuned to provide the same ponderomotive impulse, with a Gaussian radial profile ($30\ \mu\text{m}$ waist) and a central density of $1.7 \times 10^{23}\ \text{m}^{-3}$. The driver particles have the same charge as electrons, but their mass is increased to $9.1 \times 10^{-25}\ \text{kg}$ to maintain a constant ponderomotive force and steady supply of $\sim 10\ \text{MeV}$ wave breaking electrons. An example simulation can be seen in Fig 5: after 167 ps of evolution (5 cm) the giant surface wave is saturating, with 600 MV/m fields extending out to 3 mm.

We finish with 3D conformal ICEPIC calibration simulations [66, 70–75] of the D-dot probe being excited

by these surface waves, which enables the amplitude of the experimental traces to be compared with simulated SPPs. A 1 ps test wave with an E field amplitude of 1 V/m impinging upon the D-dot is found to excite a 15 μ V voltage pulse (in the 1-15 GHz band) that propagates up the coax (which is converged at a mesh resolution of 40 μ m). Adding the measured VNA transmission losses and 50 dB of attenuation reduces this to a 12 nV transient pulse at the oscilloscope. The signals recorded at $r = 10$ mm have an amplitude of 0.7 V (Fig 1), which yields a field strength of $E \sim 60$ MV/m at the D-dot. This is in nice agreement large scale axisymmetric simulations, where the surface waves have a field strength of $E \sim 145$ MV/m at $r = 10$ mm, and a duration of ~ 1 ps.

Giant surface waves excited by stable wave breaking in plasma waveguides provide an intriguing alternative use for LWFA as a source of intense THz radiation. Extrapolation from measurements, PIC simulations, and asymptotic approximations (3) converge on a surface field strength of roughly 35 GV/m, which corresponds to 1 J of THz energy, and 5% conversion efficiency from the original 800 nm laser pulse. The very high efficiency stems from the combination of the plasma waveguide effectively converting the laser pulse energy into Langmuir oscillations, which transfer a large fraction of their energy to the expelled electrons via nonlinear wave breaking, and these co-propagate coherently with a SPP, driving it to very high intensity. We are interested in directly detecting this THz radiation in future experiments, in modifying its properties by changing the laser parameters and the profile of the waveguide, and investigating out-coupling of the THz for applications.

Acknowledgments. The authors thank the Air Force Office of Scientific Research (AFOSR) for support via Laboratory Task No.s FA9550-24RDCOR002 and FA9550-22RDCOR009. This work was supported in part by high-performance computer time and resources from the DoD High Performance Computing Modernization Program. The views expressed are those of the author and do not necessarily reflect the official policy or position of the Department of the Air Force, the Department of Defense, or the U.S. government. Approved for public release; distribution is unlimited. Public Affairs release approval No. AFRL-2025-2376.

-
- [1] Donna Strickland and Gerard Mourou, "Compression of amplified chirped optical pulses," *Optics communications* **56**, 219–221 (1985).
 - [2] P Maine, D Strickland, P Bado, M Pessot, and G Mourou, "Generation of ultrahigh peak power pulses by chirped pulse amplification," *IEEE Journal of Quantum electronics* **24**, 398–403 (1988).
 - [3] JD Kmetec, JJ Macklin, and JF Young, "0.5-tw, 125-fs ti: sapphire laser," *Optics letters* **16**, 1001–1003 (1991).

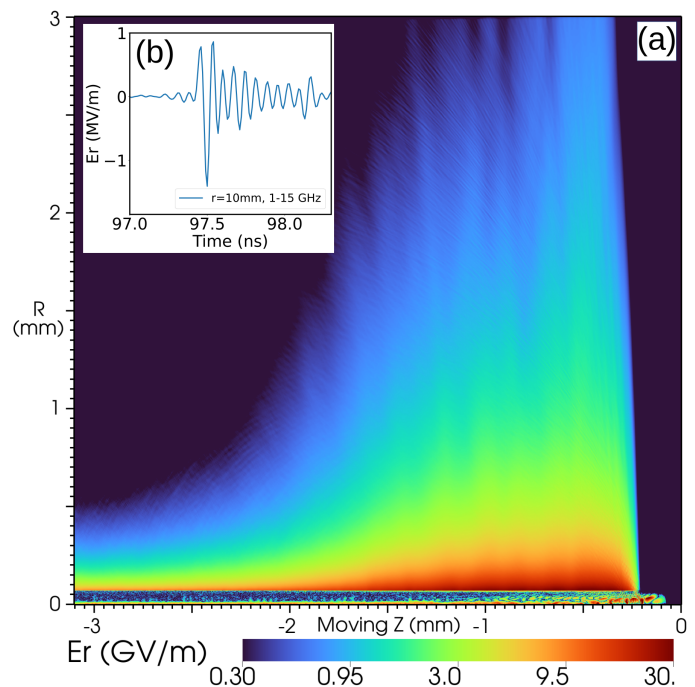


FIG. 5. (a) Log plot of E_r field strength in an axisymmetric PIC simulation which uses a sculpted particle beam to provide the ponderomotive force, leading to the same wave-breaking and surface wave excitation. The 2D r - z axisymmetry allows for much larger simulations to run much longer: the pictured wave is after 167 ps (5 cm) of propagation. (b) A measured pulse at $r = 10$ mm in the 1-15 GHz band, corrected for the 50 dB of attenuation, transmission loss and converted to electric field strength using the D-dot simulation. Extrapolation to a 1 ps pulse yields a total E field amplitude of 60 MV/m, in good agreement with simulations which show a 145 MV/m, 1 ps pulse at $r = 10$ mm.

- [4] Michael D Perry and Gerard Mourou, "Terawatt to petawatt subpicosecond lasers," *Science* **264**, 917–924 (1994).
- [5] Michael Hentschel, Reinhard Kienberger, Ch Spielmann, Georg A Reider, Nenad Milosevic, Thomas Brabec, Paul Corkum, Ulrich Heinzmann, Markus Drescher, and Ferenc Krausz, "Attosecond metrology," *Nature* **414**, 509–513 (2001).
- [6] Ferenc Krausz and Misha Ivanov, "Attosecond physics," *Reviews of modern physics* **81**, 163–234 (2009).
- [7] X Liu, D Du, and G Mourou, "Laser ablation and micromachining with ultrashort laser pulses," *IEEE journal of quantum electronics* **33**, 1706–1716 (1997).
- [8] Walter Sekundo, Kathleen S Kunert, and Marcus Blum, "Small incision corneal refractive surgery using the small incision lenticule extraction (smile) procedure for the correction of myopia and myopic astigmatism: results of a 6 month prospective study," *British Journal of Ophthalmology* **95**, 335–339 (2011).
- [9] Andrea Macchi, Marco Borghesi, and Matteo Passoni, "Ion acceleration by superintense laser-plasma interaction," *Reviews of Modern Physics* **85**, 751–793 (2013).
- [10] A Di Piazza, C Müller, KZ Hatsagortsyan, and Ch H Keitel, "Extremely high-intensity laser interactions with

- fundamental quantum systems,” *Reviews of Modern Physics* **84**, 1177 (2012).
- [11] A Fedotov, A Ilderton, F Karbstein, Ben King, D Seipt, H Taya, and Greger Torgrimsson, “Advances in qed with intense background fields,” *Physics Reports* **1010**, 1–138 (2023).
 - [12] Eric Esarey, Carl B Schroeder, and Wim P Leemans, “Physics of laser-driven plasma-based electron accelerators,” *Reviews of modern physics* **81**, 1229–1285 (2009).
 - [13] A Braun, G Korn, X Liu, D Du, J Squier, and G Mourou, “Self-channeling of high-peak-power femtosecond laser pulses in air,” *Optics letters* **20**, 73–75 (1995).
 - [14] Arnaud Couairon and André Mysyrowicz, “Femtosecond filamentation in transparent media,” *Physics reports* **441**, 47–189 (2007).
 - [15] Alfred Leitenstorfer, Andrey S Moskalenko, Tobias Kampfrath, Junichiro Kono, Enrique Castro-Camus, Kun Peng, Naser Qureshi, Dmitry Turchinovich, Koichiro Tanaka, Andrea G Markelz, *et al.*, “The 2023 terahertz science and technology roadmap,” *Journal of Physics D: Applied Physics* **56**, 223001 (2023).
 - [16] Kensuke Teramoto, Shigeki Tokita, Tokinori Terao, Shunsuke Inoue, Ryo Yasuhara, Takeshi Nagashima, Sadaoki Kojima, Junji Kawanaka, Kazuaki Mori, Masaki Hashida, *et al.*, “Half-cycle terahertz surface waves with mv/cm field strengths generated on metal wires,” *Applied Physics Letters* **113** (2018).
 - [17] Shuoting Shao, Xiangbing Wang, Rong Huang, Guangyue Hu, Min Chen, Huibo Tang, Longyu Kuang, Yuxi Liu, Yuqiu Gu, Yongkun Ding, *et al.*, “Efficiently laser driven terahertz surface plasmon polaritons on long metal wire,” *arXiv preprint arXiv:2502.08048* (2025).
 - [18] Phillip Sprangle and Eric Esarey, “Interaction of ultrahigh laser fields with beams and plasmas,” *Physics of Fluids B: Plasma Physics* **4**, 2241–2248 (1992).
 - [19] CG Durfee III and HM Milchberg, “Light pipe for high intensity laser pulses,” *Physical review letters* **71**, 2409 (1993).
 - [20] Bing Zhou, Aurélien Houard, Yi Liu, Bernard Prade, André Mysyrowicz, Arnaud Couairon, Patrick Mora, Christopher Smeenk, Ladan Arissian, and Paul Corkum, “Measurement and control of plasma oscillations in femtosecond filaments,” *Physical review letters* **106**, 255002 (2011).
 - [21] Alexander Englesbe, Jennifer Elle, Remington Reid, Adrian Lucero, Hugh Pohle, Matthew Domonkos, Serge Kalmykov, Karl Krushelnick, and Andreas Schmitt-Sody, “Gas pressure dependence of microwave pulses generated by laser-produced filament plasmas,” *Optics Letters* **43**, 4953–4956 (2018).
 - [22] Travis Garrett, Jennifer Elle, Michael White, Remington Reid, Alexander Englesbe, Ryan Phillips, Peter Mardahl, Erin Thornton, James Wymer, Anna Janicek, *et al.*, “Generation of radio frequency radiation by femtosecond filaments,” *Physical Review E* **104**, L063201 (2021).
 - [23] Travis Garrett, Anna Janicek, J Todd Fayard II, and Jennifer Elle, “Detection of surface waves during femtosecond filamentation,” *Physical Review E* **111**, 045206 (2025).
 - [24] Rufus H Ritchie, “Plasma losses by fast electrons in thin films,” *Physical review* **106**, 874 (1957).
 - [25] JM Pitarke, VM Silkin, EV Chulkov, and PM Echenique, “Theory of surface plasmons and surface-plasmon polaritons,” *Reports on progress in physics* **70**, 1 (2006).
 - [26] Toshiki Tajima and John M Dawson, “Laser electron accelerator,” *Physical review letters* **43**, 267 (1979).
 - [27] Y Ehrlich, C Cohen, A Zigler, J Krall, P Sprangle, and E Esarey, “Guiding of high intensity laser pulses in straight and curved plasma channel experiments,” *Physical review letters* **77**, 4186 (1996).
 - [28] Arthur Butler, DJ Spence, and Simon Mark Hooker, “Guiding of high-intensity laser pulses with a hydrogen-filled capillary discharge waveguide,” *Physical Review Letters* **89**, 185003 (2002).
 - [29] WP Leemans, AJ Gonsalves, H-S Mao, K Nakamura, C Benedetti, CB Schroeder, Cs Tóth, J Daniels, DE Mitchellberger, SS Bulanov, *et al.*, “Multi-gev electron beams from capillary-discharge-guided subpetawatt laser pulses in the self-trapping regime,” *Physical review letters* **113**, 245002 (2014).
 - [30] Bo Miao, Linus Feder, JE Shrock, Andrew Goffin, and HM Milchberg, “Optical guiding in meter-scale plasma waveguides,” *Physical Review Letters* **125**, 074801 (2020).
 - [31] L Feder, B Miao, JE Shrock, A Goffin, and HM Milchberg, “Self-waveguiding of relativistic laser pulses in neutral gas channels,” *Physical Review Research* **2**, 043173 (2020).
 - [32] B Miao, JE Shrock, L Feder, RC Hollinger, J Morrison, R Nedbailo, A Picksley, H Song, S Wang, JJ Rocca, *et al.*, “Multi-gev electron bunches from an all-optical laser wakefield accelerator,” *Physical Review X* **12**, 031038 (2022).
 - [33] TP Rowlands-Rees, C Kamperidis, S Kneip, AJ Gonsalves, SPD Mangles, JG Gallacher, E Brunetti, T Ibbotson, CD Murphy, PS Foster, *et al.*, “Laser-driven acceleration of electrons in a partially ionized plasma channel,” *Physical Review Letters* **100**, 105005 (2008).
 - [34] Arthur Pak, KA Marsh, SF Martins, W Lu, WB Mori, and C Joshi, “Injection and trapping of tunnel-ionized electrons into laser-produced wakes,” *Physical review letters* **104**, 025003 (2010).
 - [35] C McGuffey, AGR Thomas, W Schumaker, T Matsuoaka, V Chvykov, FJ Dollar, G Kalintchenko, V Yanovsky, A Maksimchuk, K Krushelnick, *et al.*, “Ionization induced trapping in a laser wakefield accelerator,” *Physical review letters* **104**, 025004 (2010).
 - [36] JE Shrock, E Rockafellow, B Miao, M Le, RC Hollinger, S Wang, AJ Gonsalves, A Picksley, JJ Rocca, and HM Milchberg, “Guided mode evolution and ionization injection in meter-scale multi-gev laser wakefield accelerators,” *Physical Review Letters* **133**, 045002 (2024).
 - [37] A Picksley, J Stackhouse, C Benedetti, K Nakamura, HE Tsai, R Li, B Miao, JE Shrock, E Rockafellow, HM Milchberg, *et al.*, “Matched guiding and controlled injection in dark-current-free, 10-gev-class, channel-guided laser-plasma accelerators,” *Physical Review Letters* **133**, 255001 (2024).
 - [38] E Rockafellow, B Miao, JE Shrock, A Sloss, MS Le, SW Hancock, S Zahedpour, RC Hollinger, S Wang, J King, *et al.*, “Development of a high charge 10 gev laser electron accelerator,” *Physics of Plasmas* **32**, 053102 (2025).
 - [39] WP Leemans, CGR Geddes, J Faure, Cs Tóth, J Van Tilborg, CB Schroeder, E Esarey, G Fubiani, D Auerbach, B Marcellis, *et al.*, “Observation of terahertz emission from a laser-plasma accelerated electron

- bunch crossing a plasma-vacuum boundary,” *Physical review letters* **91**, 074802 (2003).
- [40] J Déchard, A Debayle, X Davoine, L Gremillet, and L Bergé, “Terahertz pulse generation in underdense relativistic plasmas: From photoionization-induced radiation to coherent transition radiation,” *Physical Review Letters* **120**, 144801 (2018).
 - [41] J Déchard, X Davoine, and L Bergé, “Thz generation from relativistic plasmas driven by near-to far-infrared laser pulses,” *Physical Review Letters* **123**, 264801 (2019).
 - [42] Yong Wang, Shoujun Wang, Alex Rockwood, Bradley M Luther, Reed Hollinger, Alden Curtis, Chase Calvi, Carmen S Menoni, and Jorge J Rocca, “0.85 pw laser operation at 3.3 hz and high-contrast ultrahigh-intensity $\lambda=400$ nm second-harmonic beamline,” *Optics letters* **42**, 3828–3831 (2017).
 - [43] A Janicek, E Thornton, T Garrett, A Englesbe, J Elle, and A Schmitt-Sody, “Length dependence on broadband microwave emission from laser-generated plasmas,” *IEEE Transactions on Plasma Science* **48**, 1979–1983 (2020).
 - [44] AV Mitrofanov, DA Sidorov-Biryukov, MM Nazarov, AA Voronin, MV Rozhko, AB Fedotov, and AM Zheltikov, “Coherently enhanced microwave pulses from midinfrared-driven laser plasmas,” *Optics Letters* **46**, 1081–1084 (2021).
 - [45] Alexander Englesbe, Jennifer Elle, Robert Schwartz, Travis Garrett, Daniel Woodbury, Dogeun Jang, Ki-Yong Kim, Howard Milchberg, Remington Reid, Adrian Lucero, *et al.*, “Ultrabroadband microwave radiation from near-and mid-infrared laser-produced plasmas in air,” *Physical Review A* **104**, 013107 (2021).
 - [46] Erin Thornton, Travis Garrett, and Jennifer Elle, “Boosting radio frequency radiation with collisional processes in picosecond laser filamentation,” *Physics of Plasmas* **31** (2024).
 - [47] Charles K Birdsall and A Bruce Langdon, *Plasma physics via computer simulation* (CRC press, 2004).
 - [48] Roger W Hockney and James W Eastwood, *Computer simulation using particles* (crc Press, 2021).
 - [49] Arnold Sommerfeld, “Ueber die fortpflanzung elektrodynamischer wellen längs eines drahtes,” *Annalen der Physik* **303**, 233–290 (1899).
 - [50] Georg Goubau, “Surface waves and their application to transmission lines,” *Journal of Applied Physics* **21**, 1119–1128 (1950).
 - [51] Julius Adams Stratton, *Electromagnetic theory*, Vol. 33 (John Wiley & Sons, 2007).
 - [52] Sophocles J Orfanidis, “Electromagnetic waves and antennas,” (2002).
 - [53] CA Pfeiffer, EN Economou, and KL Ngai, “Surface polaritons in a circularly cylindrical interface: surface plasmons,” *Physical review B* **10**, 3038 (1974).
 - [54] Kanglin Wang and Daniel M Mittleman, “Dispersion of surface plasmon polaritons on metal wires in the terahertz frequency range,” *Physical Review Letters* **96**, 157401 (2006).
 - [55] WPEM Op ‘t Root, GJH Brussaard, PW Smorenburg, and OJ Luiten, “Single-cycle surface plasmon polaritons on a bare metal wire excited by relativistic electrons,” *Nature Communications* **7**, 13769 (2016).
 - [56] Sen Gong, Min Hu, Renbin Zhong, Xiaoxing Chen, Ping Zhang, Tao Zhao, and Shenggang Liu, “Electron beam excitation of surface plasmon polaritons,” *Optics express* **22**, 19252–19261 (2014).
 - [57] JB Andersen, “Radiation from surface-wave antennas,” *Electronics Letters* **3**, 251–252 (1967).
 - [58] Dongdong Zhang, Yafeng Bai, Yushan Zeng, Yingying Ding, Zhongpeng Li, Chuliang Zhou, Yuxin Leng, Liwei Song, Ye Tian, and Ruxin Li, “Towards high-repetition-rate intense terahertz source with metal wire-based plasma,” *IEEE Photonics Journal* **14**, 1–5 (2022).
 - [59] GI Stegeman, RF Wallis, and AA Maradudin, “Excitation of surface polaritons by end-fire coupling,” *Optics letters* **8**, 386–388 (1983).
 - [60] Serguei Y Kalmykov, Arnaud Beck, SA Yi, Vladimir N Khudik, Michael C Downer, E Lefebvre, Bradley Allan Shadwick, and DP Umstadter, “Electron self-interjection into an evolving plasma bubble: Quasimonoenergetic laser-plasma acceleration in the blowout regime,” *Physics of Plasmas* **18**, 056704 (2011).
 - [61] Benjamin R Galloway, Patrick K Rambo, Matthias Geissel, Mark W Kimmel, Jeffrey W Kellogg, Jennifer Elle, Travis Garrett, John L Porter, and Gregory A Rochau, *A study of sacrificial mirrors for use prior to a laser wake-field accelerator driven by the Z-Petawatt laser*, Tech. Rep. (Sandia National Lab.(SNL-NM), Albuquerque, NM (United States), 2022).
 - [62] J Ricardo G Mendonça, “Electromagnetic surface wave propagation in a metallic wire and the lambert w function,” *American Journal of Physics* **87**, 476–484 (2019).
 - [63] Kane Yee, “Numerical solution of initial boundary value problems involving maxwell’s equations in isotropic mdeia,” *IEEE Transactions on antennas and propagation* **14**, 302–307 (1966).
 - [64] John Villasenor and Oscar Buneman, “Rigorous charge conservation for local electromagnetic field solvers,” *Computer Physics Communications* **69**, 306–316 (1992).
 - [65] Jay P Boris, “Relativistic plasma simulation-optimization of a hybrid code,” in *Proc. Fourth Conf. Num. Sim. Plasmas* (1970) pp. 3–67.
 - [66] Robert E Peterkin and John W Luginsland, “A virtual prototyping environment for directed-energy concepts,” *Computing in Science & Engineering* **4**, 42–49 (2002).
 - [67] Bo Miao, Ela Rockafellow, JE Shrock, SW Hancock, Daniel Gordon, and HM Milchberg, “Benchmarking of hydrodynamic plasma waveguides for multi-gev laser-driven electron acceleration,” *Physical Review Accelerators and Beams* **27**, 081302 (2024).
 - [68] John M Dawson, “Nonlinear electron oscillations in a cold plasma,” *Physical review* **113**, 383 (1959).
 - [69] SV Bulanov, Francesco Pegoraro, AM Pukhov, and AS Sakharov, “Transverse-wake wave breaking,” *Physical review letters* **78**, 4205 (1997).
 - [70] DE Merewether, R Fisher, and FW Smith, “On implementing a numeric huygen’s source scheme in a finite difference program to illuminate scattering bodies,” *IEEE Transactions on Nuclear Science* **27**, 1829–1833 (1980).
 - [71] Allen Taflov and Susan C Hagness, *Computational electrodynamics: the finite-difference time-domain method* (Artech house, 2005).
 - [72] IA Zagorodnov, Rolf Schuhmann, and Thomas Weiland, “A uniformly stable conformal fdtd-method in cartesian grids,” *International Journal of Numerical Modelling: Electronic Networks, Devices and Fields* **16**, 127–141 (2003).
 - [73] Tian Xiao and Qing Huo Liu, “A 3-d enlarged cell technique (ect) for the conformal fdtd method,” *IEEE trans-*

- actions on antennas and propagation **56**, 765–773 (2008).
- [74] Gregory Koidze, “Implementation of collocated surface impedance boundary conditions in fdtd,” *IEEE transactions on antennas and propagation* **58**, 2394–2403 (2010).
- [75] Jean-Pierre Berenger, “A perfectly matched layer for the absorption of electromagnetic waves,” *Journal of computational physics* **114**, 185–200 (1994).